1

2

Supporting Information for

3

First-order River Delta Morphology is set by the Sediment Flux Balance from Rivers, Waves, and Tides

4
5

C. M. Broaddus[1,2], L. M. Vulis[2], J. H. Nienhuis[3], A. Tejedor[2,4], J. Brown[1], E. Foufoula-Georgiou[2,5], D. A. Edmonds[1]

[1]Department of Earth and Atmospheric Sciences, Indiana University, Bloomington, IN, USA, [2]Department of Civil and Environmental Engineering, University of California, Irvine, CA, USA, [3]Department of Physical Geography, Utrecht University, Utrecht, NL, [4]Department of Science and Engineering, Sorbonne University, Abu Dhabi, UAE, [5]Department of Earth System Science, University of California, Irvine, CA, USA

6
7

8
9
10
11

12

Contents of this file

13
14

Text S1 to S3
Figures S1 to S4
Tables S2, S4 to S6

15
16
17

18

Additional Supporting Information (Files uploaded separately)

19
20

Tables S1, S3

21

22

Introduction

23

This file contains supporting information (text, figures, tables) concerning the model setup, model sensitivity testing, and compilation of the field delta dataset. We also include morphometric results for all simulated and field deltas as tables, as well as the results of our various statistical hypothesis tests (as a table). Finally, we include a figure showing the depth outputs of a number of model runs with "intermediate" forcing balances.

24
25
26
27
28
29

30

Text S1 - Model Setup

We developed a suite of numerically simulated river deltas using the hydro-morphodynamic model Delft3D. Delft3D can reproduce coastal and deltaic hydrodynamics and has been used extensively to simulate the morphological evolution of river deltas at timescales ranging from decades to centuries (Caldwell & Edmonds, 2014; Edmonds & Slingerland, 2007; Geleynse et al., 2011; Rossi et al., 2016). Our models use the depth-averaged, Reynolds-averaged Navier-Stokes equations for incompressible free-surface flow (shallow water equations), coupled with the SWAN model for wave energy propagation and dissipation. A detailed description of the governing equations and solution scheme can be found in the Delft3D user manual ("Delft3D-FLOW User Manual," n.d.).

The flow equations are solved on a rectilinear grid of 25 x 25 meter cells (Figure S1a). We model a river entering a basin (9000 m in cross-shore direction and 21000 m in longshore direction) in the presence of waves and tides, ignoring the effects of salinity and base-level change. Our flow domain includes an elongated feeder channel (width = 450 m, length = 59900 m) that extends upstream from the basin, the purpose of which is to prevent the tidal hydrodynamics in the basin from affecting the upstream boundary (Figure S1b).

All runs use a computational time step of 30 seconds. We apply a morphological scaling factor of 180 to speed up bed adjustments and decrease computational time for the runs, assuming that bed relaxation is negligible at the modeled timescales. Initial bathymetry in the feeder channel is trapezoidal in cross section and slopes linearly ($S \sim 10^{-4}$) toward the basin. Cross shore bathymetry in the basin follows a power law curve similar to the Dean profile (Dean, 1991), modified here to produce a shallower platform to allow for faster progradation (Figure S1c). This profile reduces cross shore transport and morphological "spin-up" associated with adjustment of the shoreface to the wave climate. We also apply a random roughness (amplitude = 0.01 meter) to the initial bathymetric surface to simulate natural variations in the bed topography. Initial sediment thickness is 5 meters throughout the domain.

At the upstream boundary, we specify a steady incoming water discharge of 1250 m^3s^{-1} carrying a non-cohesive sediment load of uniform grain size (135 microns) at a concentration that is in equilibrium with the hydrodynamics at the boundary. We calculate sediment transport according to the Soulsby and Van Rijn equation from Delft3D ("Delft3D-FLOW User Manual," n.d.; Soulsby, 1997) because it is capable of handling waves. Our use of an equilibrium sediment concentration at the upstream boundary (see Text S1) complicates an a priori sediment flux estimate; instead, we extract the time-averaged Q_{river} value for each model run directly from a cross-section located near the upstream boundary.

In the basin, we specify a harmonic water-level condition at the northern boundary, representing tides with a frequency of 30 degrees per hour and a constant amplitude (ranges from 0 – 2 meters depending on simulation) (Figure S1e). Neumann boundaries are used along the eastern and western edges of the basin, allowing water and sediment to move freely into and out of the domain. Additional significant model variables are listed with their specified values in Table S5. Notably, we use the default value for the

75 transverse bed slope parameter because small changes in the value of this parameter
76 have been shown to have a large effect on morphology (Baar et al., 2019).
77   Wave equations are solved on a separate, larger domain that overlaps the flow
78 domain (Figure S1a). The larger wave domain allows boundary effects to spatially
79 dissipate prior to wave interaction with the flow model. The wave grid has a variable
80 resolution to facilitate faster computational times: areas overlapping the flow domain
81 have square 50 x 50 meter cells while all other areas have rectangular, 200 x 50 meter
82 grid cells. Coupling between the flow and wave domains occurs at a regular interval (120
83 simulation minutes). Boundaries are placed along the North, East, and West edges of the
84 wave domain, and impart significant wave heights ranging from 0 - 3 meters at a
85 frequency of 5 seconds (Figure S1d). Wave amplitude varies between runs but is constant
86 throughout a given run. Wave direction randomly varies between -45, -30, 30, and 45
87 degrees relative to shore normal throughout the run, but the directional (and temporal)
88 distribution of wave energy is constant for all runs (Figure S1d). For stability reasons, we
89 allow the hydrodynamics in the flow model to spin-up for 12 hours (in hydrodynamic
90 time) prior to initiation of wave coupling and morphodynamic adjustment.
91   As with all models there are limitations inherent to our schematization. Delft3D uses
92 a simplified scheme for the erosion of dry cells whereby an "erosion factor" is applied to
93 dry cells adjacent to wet cells experiencing erosion (dry cell erosion = erosion factor *
94 wet cell erosion). This scheme is effective at allowing channels to migrate and avulse to
95 new locations, but seems to inhibit their ability to adjust their width in response to
96 changes in hydrodynamics at the river mouth. As a result, our models do not reproduce
97 the increase in river mouth width with tidal-dominance predicted by Nienhuis et al.
98 (2018). Adjusting the dry cell erosion factor does not have a significant effect on the
99 channel width at the river mouth. See Text S2 for details on simple sensitivity tests that
100 were performed to test the robustness of our results to the selection of computational
101 parameters.
102   The model is not designed to represent specific delta conditions but instead to have
103 characteristics (boundary and initial conditions) representative for a wide swath of river
104 deltas. Certain processes are excluded from the model (salinity and density differences,
105 vegetation, permafrost, etc.) based on the assumption that their effects on morphology
106 are second order. Other factors known to affect morphology (sediment grain size and
107 cohesion, basin bathymetry) are intentionally held constant to keep the analysis focused
108 on the role of sediment flux balance. Thus, the overall interpretation of model results
109 relies on the assumption that these factors, while important in determining the overall
110 morphology of an individual delta, do not change the nature of the flux balance -
111 morphology relationships discussed here.
112   Specifically, we use a set of steady state boundary conditions, assuming that
113 seasonal variability in discharge and environmental forcings is less important than the
114 net sediment flux balance. We assume the morphodynamics of non-cohesive delta
115 systems can be adequately modeled with a single sediment fraction in both the bed and
116 the flow. Adjustments to the standard deviation of the grain size distribution have been
117 shown to have little effect on the morphologic output of Delft3D models (Caldwell and
118 Edmonds (2014)).

119   Interpreting the temporal scale (and consequently the spatial scale) of the
120   simulations in terms of real-world time-space scales is complicated. Our simulations run
121   for 31 days of constant river discharge and wave energy. Multiplying by the total
122   simulation time by the morphological scale factor would suggest that the simulations
123   model ~15 years of delta evolution. However, considering that the majority of
124   geomorphic work occurs during periods of high flow and/or wave energy, and that our
125   simulations evolve under a constant river discharge and constant wave energy, the
126   results can be thought of as representing a "fast-forwarded" version of delta growth.
127   Interpreting the results in this manner relies on an assumption of intermittently effective
128   wave transport with timescales similar to that of the fluvial system, which is unlikely in
129   continental scale systems where catchment and shoreline conditions are largely
130   decoupled (tidal prism here depends on fluvial discharge and thus is coupled). Instead,
131   the results are better interpreted based on the fundamental behaviors that they reveal
132   regarding the interaction of forcing and morphology in the simplest case imaginable.
133

134   **Text S2** - Model sensitivity tests
135   To assess the robustness of our model results to user-defined computational
136   parameters, we developed a suite of test runs that vary in computational timestep, wave-
137   flow coupling interval, and morphological scale factor. Each test holds all other
138   parameters constant. Morphological scale factor (MSF) and computational timestep (DT)
139   tests were performed using a river dominated simulation, while the coupling interval test
140   was performed using a wave dominated simulation. While the results of each test do
141   vary slightly in terms of their channel networks and shoreline structure (Figure S4), the
142   differences are within the range of morphological variability observed for a given flux
143   balance. Also, for each parameter tested the range of Nch and r* values between runs is
144   less than the temporal variance (over the final 1/3 of the simulation duration) in the
145   metric values for those runs (Table S6)."
146

147   **Text S3** - Field delta dataset
148   We use a set of field deltas to cover the variety of flux values observed in nature
149   (Figure 1b, Table S3). Our dataset is modified from the dataset of Syvitski and Saito
150   (2007) with some deltas added from Caldwell et al. (2019) to increase coverage of
151   parameter space. End-member and axial coverage is already significant within the
152   Syvitski and Saito (2007) dataset, so we selected only deltas from Caldwell et al. (2019)
153   with mixed flux balances (no single flux >90%). We also excluded deltas that were heavily
154   modified by humans, and deltas with catchment areas lower than the median value in
155   the dataset (as these deltas skew heavily toward wave-dominance). The final compiled
156   dataset consists of 78 globally-distributed river deltas that span climate zones and
157   catchment types.
158   Field deltas are positioned in ternary space according to their flux values as
159   reported by Nienhuis et al. (2020) (Version 1.0). We used the "pristine" fluvial sediment
160   flux values to represent Q_{river}. As with any global dataset, there is significant uncertainty
161   in the flux values for any single delta (discussed more thoroughly in the source
162   publication). The largest source of this uncertainty lies in the fluvial sediment flux values;

163   the WBMSed model from which these values are sourced excludes bedload sediment
164   entirely and has an average R^2 of ~0.65 for annual suspended sediment flux predictions.
165   Another source of uncertainty in the flux values is the spatial ambiguity of wave and tidal
166   conditions sourced from global datasets. While the uncertainty in these factors can at
167   times be significant, the predicted sediment flux values are not expected to be
168   systematically biased in a manner that would affect the relationships discussed here. See
169   Nienhuis et al (2020) for a more detailed discussion of the uncertainty in these values.
170   For each delta we obtained pre-compiled 1984-2019 water surface occurrence
171   products from the Global Surface Water dataset of Pekel et al. (2016). We used the delta
172   area polygons of Edmonds et al. (2020) to determine the extent of the occurrence image
173   for each delta. However, the extent of these polygons is in some cases too small and
174   does not fully enclose the delta shoreline. We addressed this by isotropically increasing
175   the area of each polygon by 21%, which is equivalent to a 10% increase in the diameter
176   of a circle of the same area.
177   To avoid scale-dependent differences in ρ* between large and small deltas, each
178   compiled occurrence map is resampled to have the same relative resolution as the
179   smallest delta in the dataset. The relative resolution is determined by dividing the area of
180   1 pixel by the area of the bounding box for the smallest delta in the dataset. We obtain
181   binary wet or dry maps for each delta by applying a threshold to the resampled
182   compiled occurrence products. We assume the deltas did not experience significant
183   system-scale morphological change between 1984-2019 and choose a threshold value of
184   50% to smooth over occurrence differences due to tidal inundation. The binarized
185   occurrence maps are used in conjunction with the opening angle method of Shaw et al.
186   (2008) to define the 45- and 120-degree shorelines for each field delta.
187   We use the occurrence maps and shorelines to calculate the morphological metrics
188   for the field delta dataset. ρ* and S_{PA} are determined following a methodology identical
189   to the simulations. For ρ* and S_{PA}, we remove deltas with significant human modification
190   to the shoreline, defined here as deltas where >10% of the shoreline length has been
191   anthropogenically-straightened via dikes or seawalls (noted in Table S3). We also exclude
192   deltas where humans have controlled and significantly disrupted the avulsion cycle (and
193   thus the shoreline morphology), including the Mississippi and the Yellow River deltas.
194   For the number of channel mouths metric, we use the values reported by Syvitski
195   and Saito (2007) where available and follow their methodology to count the number of
196   channel mouths for deltas in the Caldwell et al. (2019) dataset. We use the occurrence
197   products in conjunction with satellite imagery for these channel mouth counts. We
198   exclude deltas with significant anthropogenic modification to the distributary network,
199   which we define as deltas where greater than ~10% of the total combined distributary
200   length (from apex to shoreline) has been straightened or visibly modified when viewed at
201   the scale of the entire delta.
202
203
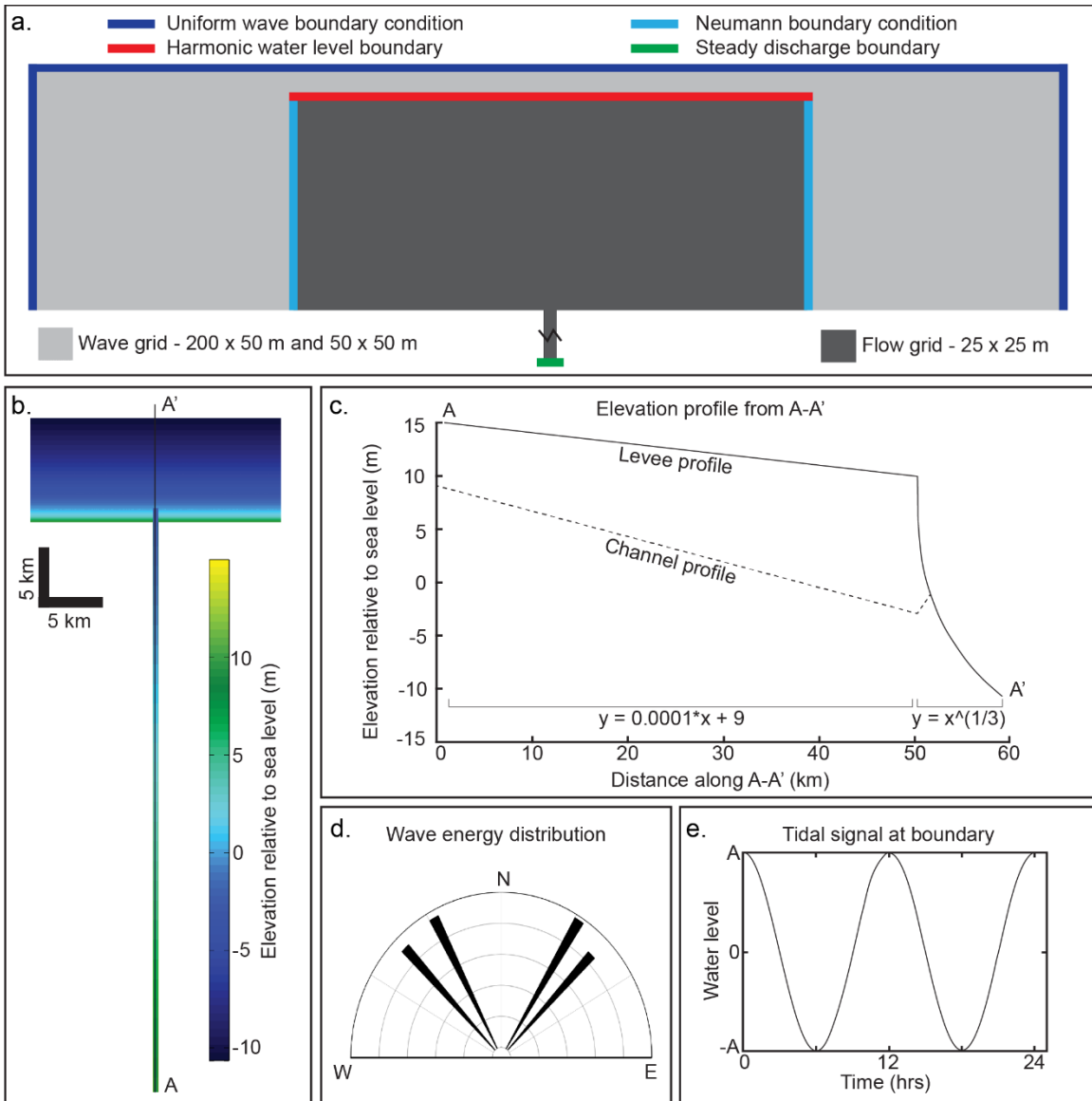
204
205 **Figure S1: Schematics illustrating model setup**. (A) Truncated flow and wave domains.
206 (B) Full flow domain. (C) Initial bathymetry for flow domain. (D) Distribution of wave
207 energy at wave domain boundaries. (E) Tidal signal at harmonic boundary condition.
208
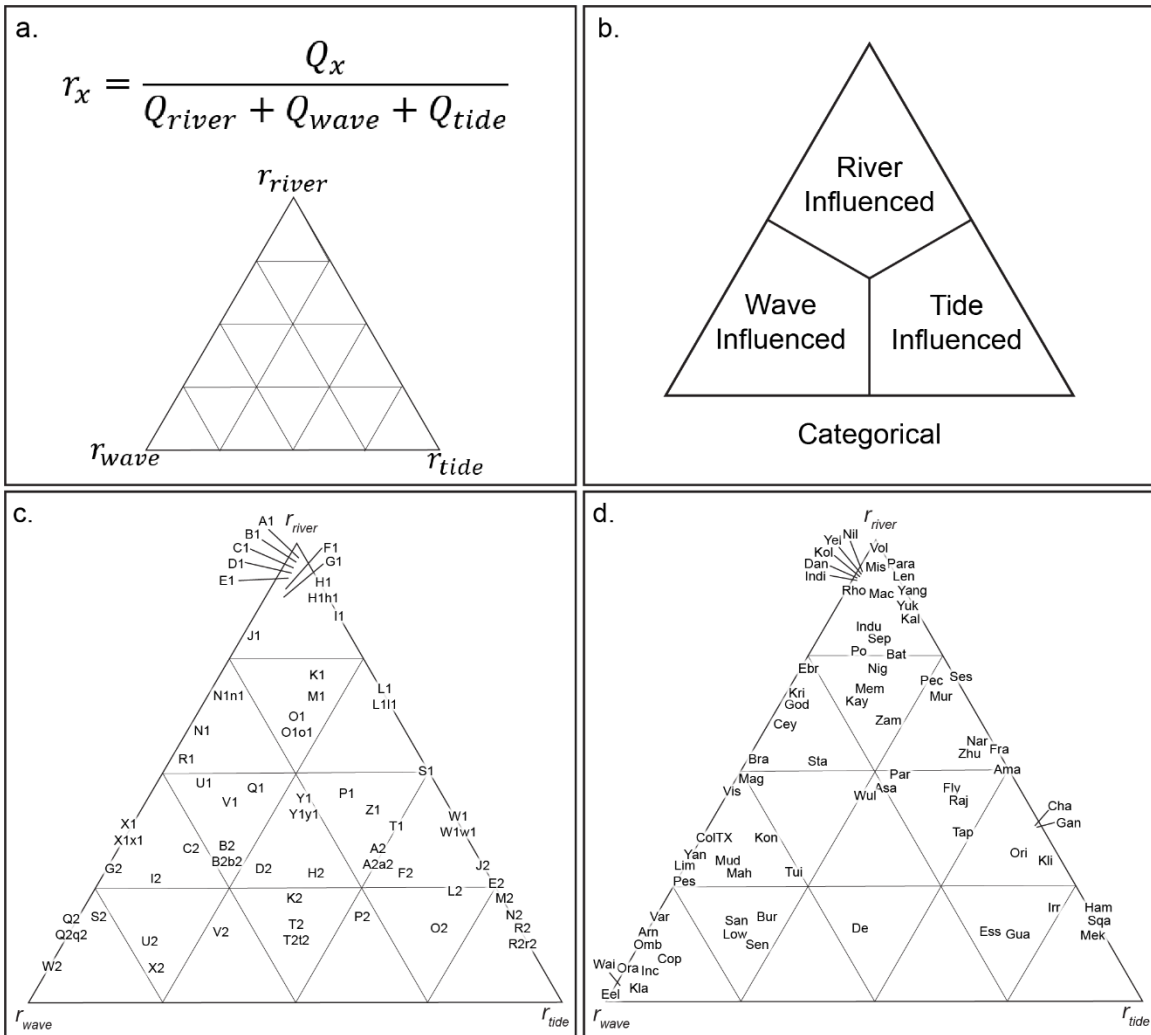
Figure S2: Ternary space schematics and delta locations in ternary space. (a) Ternary diagram schematic and equation defining plotting locations in ternary space as a function of flux balance at the river mouth. (b) Categorical schematic of ternary space defining boundaries of different categories. (c,d) Ternary diagrams showing the locations of the 62 simulations (c) and 78 field deltas (d) referenced in this paper. Abbreviations in (c) and (d) correspond to abbreviations in Table S1 and Table S3.
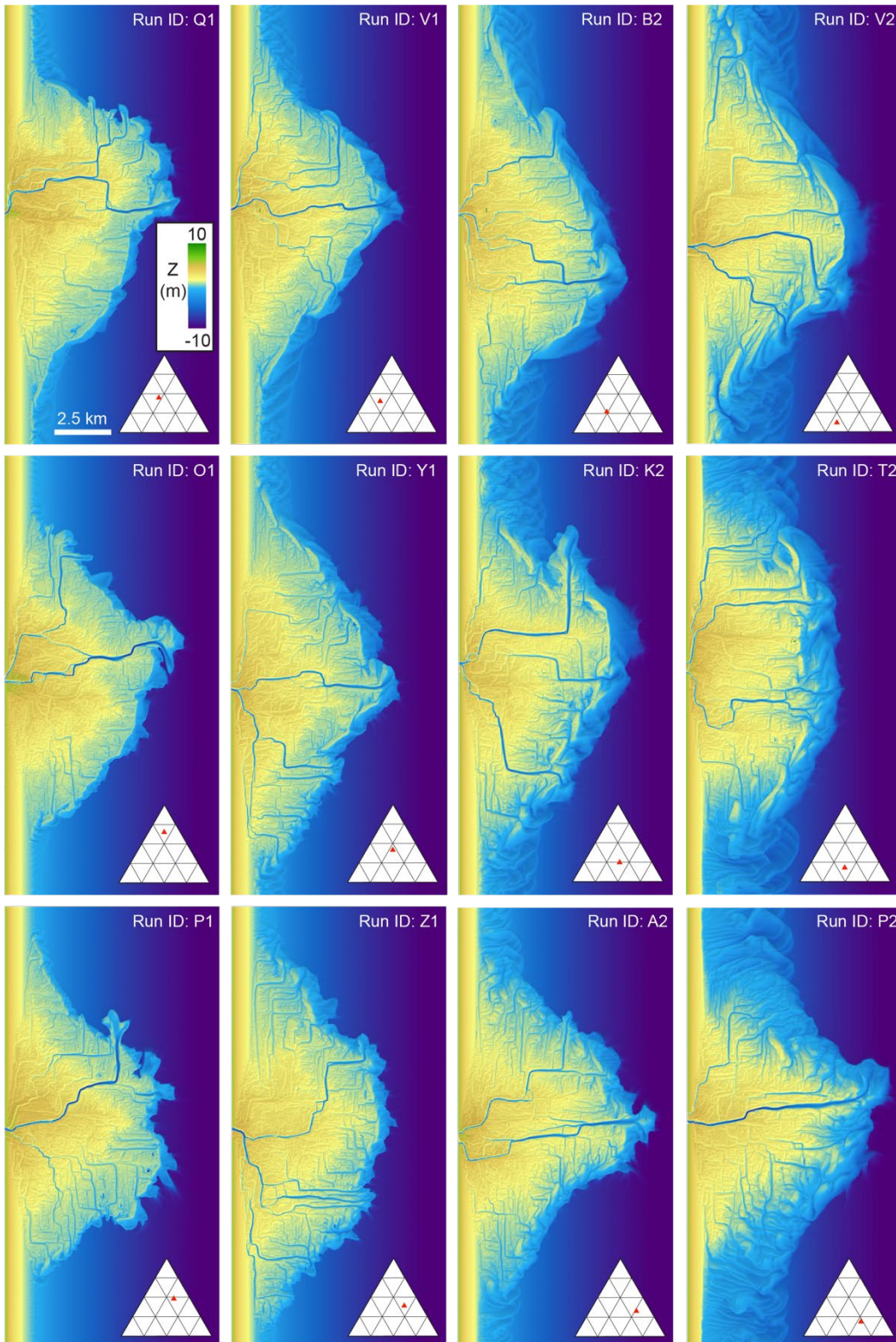
217
218 **Figure S3: Representative set of simulations with intermediate flux balances.** Color
219 bar represents elevation in meters above sea level and applies to all images (scale bar
220 also applies to all images).
221
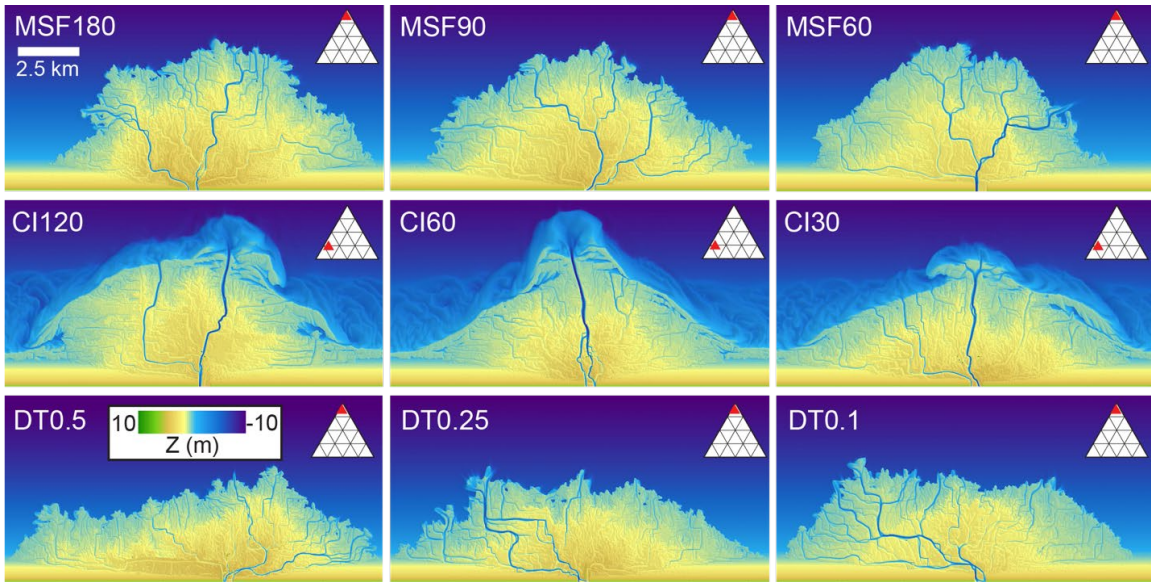
Figure S4: Morphological outputs from sensitivity tests. Each row shows the outputs from a different sensitivity test: row 1 varies the morphological scale factor between 60 and 180, row 2 varies the flow/wave coupling interval from 30 to 120 minutes, and row 3 varies the computational timestep from 0.1 to 0.5 min. The color and scale bars apply to all panels.
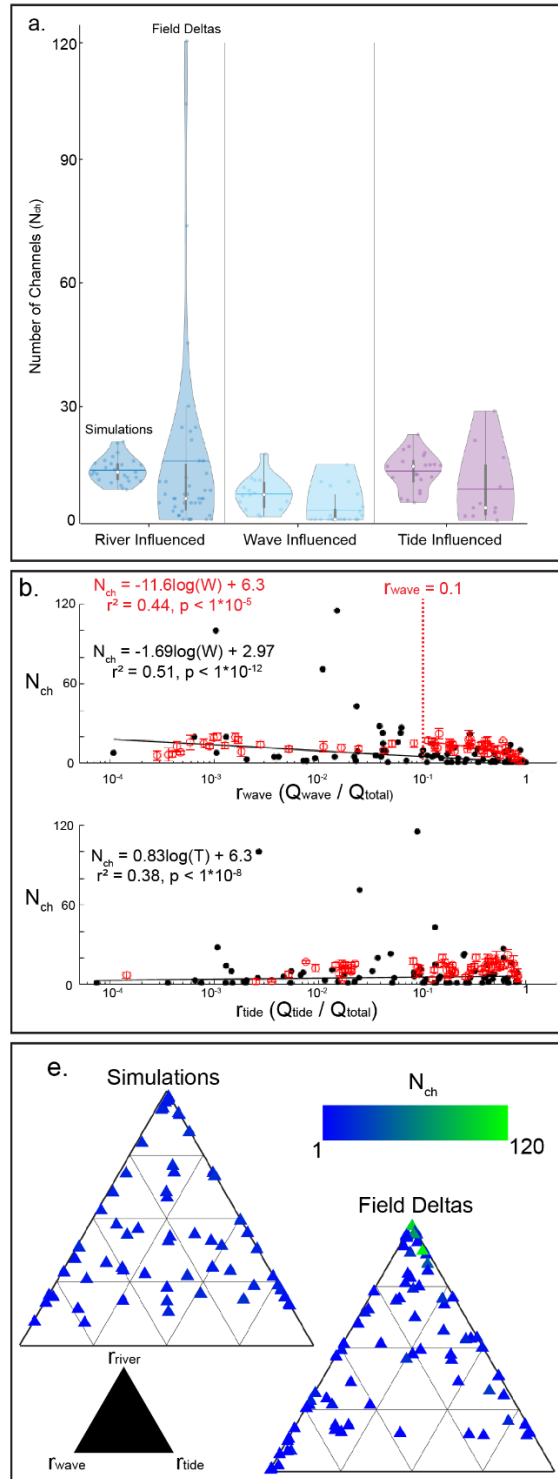
229
230
Figure S5: N$_{ch}$ trends including deltas with N$_{ch}$ > 30. (a) Categorical, (b)
dominance based, and (c) ternary distributions of the number of distributary
channels for simulated and global deltas.
234

RunID	SWH (m)	Ta (m)	Qriver (kg/s)	Qwave (kg/s)	Qtide (kg/s)	Q (m^3/s)	Nch	Standard deviation (Nch)	ρ*	Standard deviation (ρ*)	SPA (0/1 = absent/present)
A1	0.12	0.01	134.82695	0.4	2.4	1250	14.0	2.75	1.253	0.02	0
B1	0.15	0.01	122.32964	0.7	2.4	1250	10.8	2.25	1.241	0.05	0
C1	0.2	0.01	112.10652	1.3	2.4	1250	12.5	3.69	1.212	0.02	0
D1	0.25	0.01	129.36682	2.2	2.4	1250	11.7	2.98	1.236	0.01	0
E1	0.3	0.01	134.87795	3.5	2.4	1250	11.1	1.91	1.315	0.02	0
F1	0.35	0.01	108.45752	5.0	2.4	1250	9.7	1.70	1.331	0.03	0
G1	0.4	0.01	124.71297	6.9	2.4	1250	14.9	2.47	1.258	0.04	0
H1	0.1	0.05	123.48067	0.2	12.2	1250	8.8	3.4	1.372	0.03	0
H1h1	0.1	0.05	134.16706	0.2	12.2	1250	17.6	2.17	1.372	0.03	0
I1	0.1	0.1	130.80986	0.2	24.5	1250	19.9	3.18	1.295	0.03	0
J1	0.7	0.01	114.82952	26.5	2.4	1250	15.6	3.31	1.185	0.01	0
K1	0.6	0.1	103.85743	18.3	24.5	1250	16.6	2.72	1.213	0.03	0
L1	0.1	0.25	132.38436	0.2	62.1	1250	13.5	2.64	1.439	0.03	0
L1l1	0.09	0.24	120.06927	0.2	59.6	1250	20.2	2.82	1.371	0.03	0
M1	0.7	0.15	135.9678	26.5	36.9	1250	12.4	2.76	1.269	0.02	0
N1	1	0.01	98.856738	62.5	2.4	1250	14.7	1.77	1.204	0.01	1
N1n1	1.01	0.02	145.27914	64.0	4.9	1250	15.7	1.70	1.150	0.02	1
O1	0.9	0.2	137.05152	48.5	49.5	1250	9.0	3.16	1.179	0.03	0
O1o1	0.89	0.19	143.84584	47.2	47.0	1250	14.7	1.70	1.164	0.01	1
P1	0.8	0.3	87.083916	36.6	74.9	1250	11.7	2.11	1.217	0.04	0
Q1	1.1	0.15	98.047277	78.5	36.9	1250	10.4	5.36	1.118	0.03	1
R1	1.3	0.01	136.39073	117.3	2.4	1250	12.2	2.82	1.169	0.02	1
S1	0.1	0.5	123.48463	0.2	127.0	1250	19.4	2.37	1.425	0.03	0
T1	0.7	0.45	90.75452	26.5	113.8	1250	17.3	2.06	1.243	0.03	0
U1	1.3	0.1	128.55421	117.3	24.5	1250	12.9	2.02	1.185	0.04	1
V1	1.4	0.2	146.73721	140.1	49.5	1250	15.0	1.83	1.149	0.02	1
W1	0.1	0.75	118.85713	0.2	194.6	1250	15.1	3.18	1.458	0.02	0
W1w1	0.11	0.74	153.01358	0.3	191.9	1250	12.9	1.85	1.404	0.03	0
X1	1.6	0.01	122.69353	193.0	2.4	1250	17.0	1.15	1.150	0.01	1
X1x1	1.61	0.02	103.91654	195.9	4.9	1250	8.3	1.34	1.109	0.01	1
Y1	1.2	0.4	137.21305	96.8	100.7	1250	13.0	2.40	1.188	0.02	1
Y1y1	1.19	0.41	147.83408	94.9	103.3	1250	10.8	2.57	1.218	0.02	1
Z1	0.9	0.6	141.76731	48.5	153.7	1250	11.6	3.66	1.233	0.03	1
A2	1.1	0.8	127.06515	78.5	208.5	1250	12.2	3.88	1.311	0.02	1
A2a2	1.11	0.81	127.81321	80.3	211.3	1250	12.1	4.15	1.242	0.02	1
B2	1.7	0.35	136.18492	223.3	87.7	1250	10.8	1.75	1.127	0.03	1
B2b2	1.69	0.36	129.70471	220.1	90.3	1250	9.0	3.30	1.152	0.03	1
C2	1.8	0.25	152.41589	256.1	62.1	1250	10.8	1.87	1.129	0.01	1
D2	1.6	0.5	124.63476	193.0	127.0	1250	7.3	2.26	1.144	0.02	1
E2	0.1	1.2	100.22115	0.2	323.3	1250	15.9	5.78	1.440	0.04	0
F2	1	1	135.90333	62.5	265.0	1250	14.7	3.92	1.388	0.02	0
G2	2	0.01	133.83115	329.8	2.4	1250	7.7	2.45	1.131	0.01	1
H2	1.4	0.8	131.05558	140.1	208.5	1250	18.7	4.42	1.281	0.02	1
I2	2	0.2	133.82084	329.8	49.5	1250	11.2	3.05	1.140	0.02	1
J2	0.1	1.4	142.25744	0.2	383.4	1250	8.2	1.32	1.376	0.02	0
K2	1.6	0.75	113.92028	193.0	194.6	1250	8.9	1.20	1.262	0.03	1
L2	0.9	1.3	134.94537	48.5	393.9	1250	15.2	2.68	1.388	0.04	0
M2	0.1	1.6	123.52444	0.2	445.2	1250	12.7	3.68	1.395	0.04	0
N2	0.1	1.8	118.42871	0.2	508.8	1250	7.0	2.40	1.343	0.02	0
O2	1.2	1.6	118.92084	96.8	445.2	1250	22.3	3.74	1.569	0.07	0
P2	1.6	1.3	137.87433	193.0	353.1	1250	17.9	7.14	1.441	0.04	0
Q2	2.5	0.01	114.00578	563.4	2.4	1250	2.5	0.97	1.117	0.02	1
Q2q2	2.49	0	136.71441	558.0	0.1	1250	7.1	2.38	1.143	0.01	1
R2	0.1	2	110.67468	0.2	574.2	1250	6.6	5.04	1.373	0.03	0
R2r2	0.09	2.01	106.66411	0.2	577.5	1250	6.1	3.41	1.454	0.02	0
S2	2.5	0.05	134.79892	563.4	12.2	1250	3.8	1.69	1.122	0.02	1

T2	1.9	1.1	122.75985	291.6	293.9	1250	14.9	4.09	1.301	0.07	1
T2t2	1.89	1.11	88.642066	287.9	296.9	1250	15.0	4.92	1.388	0.03	1
U2	2.4	0.35	99.439763	510.8	87.7	1250	3.8	2.25	1.131	0.04	1
V2	2.2	0.75	129.45124	414.5	194.6	1250	5.7	1.70	1.188	0.02	1
W2	3	0.01	88.642659	872.6	2.4	1250	2.1	1.45	1.122	0.02	1
X2	3	0.8	105.2153	872.6	208.5	1250	5.6	1.08	1.159	0.05	1

235

236 **Table S1.** List of simulations developed in this study including key parameters and
237 morphological metric values.

238
239
240
241

Metric	Group A	Group B	P-value	Significant? (Y/N)
Roughness (ρ^*) (Simulations)	River-influenced	Wave-influenced	$1*10^{-3}$	Y
	River-influenced	Tide-influenced	$2*10^{-3}$	Y
	Wave-influenced	Tide-influenced	$<1*10^{-4}$	Y
Roughness (ρ^*) (Global deltas)	River-influenced	Wave-influenced	$1.1*10^{-2}$	Y
	River-influenced	Tide-influenced	0.14	N
	Wave-influenced	Tide-influenced	$1*10^{-3}$	Y
Number of Distributary Channels (N_{ch}) (Simulations)	River-influenced	Wave-influenced	$3*10^{-4}$	Y
	River-influenced	Tide-influenced	0.99	N
	Wave-influenced	Tide-influenced	$4*10^{-4}$	Y
Number of Distributary Channels (N_{ch}) (Global deltas)	River-influenced	Wave-influenced	$2*10^{-4}$	Y
	River-influenced	Tide-influenced	0.83	N
	Wave-influenced	Tide-influenced	$5*10^{-2}$	Y

242 **Table S2.** Categorical pairwise comparison summary

243

Delta ID	Name	Qriver (kg/s)	Qwave (kg/s)	Qtide (kg/s)	QH2O (m^3/s)	SWH (m)	Ta (m)	Latitude (DD)	Longitude (DD)	Dataset	Nch	SPA	ρ*
Ama	Amazon	31142	66	30857	138530	0.38	1.10	-0.667	308.921	SS2007	8	0	1.627
Cey	Ceyan	315	205	6	112	0.58	0.14	36.571	35.563	SS2007	3	1	1.27
ColMX	Colorado, MX	7722	120	450	234	0.50	2.10	31.921	245.046	SS2007	5	0	1.2
Cop	Copper	343	3681	139	1290	1.87	1.37	60.446	215.150	SS2007	10	1	1.372
Dan	Danube	4295	204	33	4210	0.94	0.02	45.250	29.700	SS2007	9	1	1.178
Ebr	Ebro	703	259	2	160	0.79	0.07	40.721	360.854	SS2007	3	1	1.209
Eel	Eel, CA	76	8331	17	227	2.50	0.91	40.625	235.721	SS2007	1	1	1.009
Fly	Fly	2586	689	2189	4992	0.82	0.28	-8.275	142.404	SS2007	5	0	1.563
Gan	Ganges-Brahmaputra	53453	181	84709	38181	0.53	0.79	23.225	90.633	SS2007	20	0	1.719
God	Godavari	3337	1781	71	4324	1.49	0.46	16.713	82.246	SS2007	11	1	1.224
Indi	Indigirka	1914	78	2	594	0.56	0.02	71.550	150.750	SS2007	28	1	1.236
Indu	Indus	24097	3409	2551	5137	1.69	1.11	24.083	67.654	SS2007	6	1	1.503
Irr	Irriwaddy	10031	2902	36473	12676	1.48	0.88	16.363	95.042	SS2007	16	1	1.244
Kol	Kolyma	2591	114	15	1524	0.64	0.03	69.527	161.383	SS2007	10	0	1.308
Kri	Krishna	2423	1195	66	2712	1.30	0.42	15.763	80.838	SS2007	7	1	1.153
Lim	Limpopo	879	2383	18	88	1.99	0.73	-25.171	33.517	SS2007	1	1	1.034
Mac	MacKenzie	4320	304	244	7031	0.88	0.13	69.450	225.850	SS2007	23	0	1.252
Mah	Mahanadi	1384	3307	429	2494	1.30	0.67	20.333	86.658	SS2007	9	1	1.123
Mek	Mekong	15737	2627	90814	16361	1.59	1.56	9.617	106.254	SS2007	9	0	1.266
Nig	Niger	13654	2314	2481	8700	1.21	0.59	4.396	6.071	SS2007	15	1	1.108
Nil	Nile	33631	1255	163	7669	1.32	0.10	31.446	30.388	SS2007	6	1	1.069
Ora	Orange	710	9652	4	45	2.55	0.54	-28.629	16.454	SS2007	1	1	1.044
Ori	Orinoco	19594	3804	36549	34074	1.85	0.59	8.579	299.021	SS2007	27	1	1.342
Para	Parana	8203	6	322	26530	0.16	0.09	-33.933	301.479	SS2007	20	0	1.464
Po	Po	960	177	120	813	0.73	0.28	44.963	12.517	SS2007	7	1	1.189
Son	Song Hong	2590	466	1482	2485	0.84	0.94	20.317	106.533	SS2007	10	1	1.365
Vis	Vistula	721	825	1	311	1.20	0.01	54.313	18.938	SS2007	3	1	1.001
Vol	Volga	4682	5	13	7538	0.17	0.01	45.596	47.721	SS2007	100	0	1.508
Yan	Yana	926	2319	4	360	1.58	0.25	71.534	136.550	SS2007	14	1	1.142
Yang	Yangtze	6098	65	765	19898	0.64	0.33	31.942	120.238	SS2007	4	0	1.472
Yuk	Yukon	3308	93	527	4022	0.65	0.51	63.040	195.536	SS2007	43	0	1.213
Asa	Asahan	92	50	52	214	0.34	1.16	2.971	99.813	Cea2019	1	0	1.044
Bat	Batanghari	1067	141	214	1863	0.64	0.64	-1.096	104.192	Cea2019	6	0	1.089
Bur	Burhabalanga / Karkai	147	497	146	388	0.70	1.40	21.592	87.308	Cea2019	1	1	1.094
De	De Grey	53	159	131	13	0.69	2.14	-20.000	119.175	Cea2019	1	1	1.05
Ess	Essequibo	758	1137	3169	3827	1.04	0.79	6.450	301.408	Cea2019	4	0	1.626
Inc	Incomati	172	1942	49	37	1.85	0.74	-25.767	32.733	Cea2019	2	1	1.342
Kal	Kalimantan	1292	58	236	5400	0.39	0.58	-0.137	109.192	Cea2019	6	0	1.222
Kay	Kayan	476	144	67	1570	0.48	0.75	2.925	117.608	Cea2019	12	0	1.516
Kon	Konkoure	253	374	74	536	0.66	1.28	9.950	346.313	Cea2019	2	1	1.365
Low	Lower Savannah	216	896	190	214	1.23	0.83	32.075	279.029	Cea2019	4	1	1.1
Mem	Memberamo	3711	1020	557	4340	1.18	0.54	-1.592	137.867	Cea2019	1	1	1.082
Mud	Muda	54	120	10	156	0.43	0.81	5.571	100.350	Cea2019	1	1	1.069
Mur	Murung	681	48	278	3393	0.36	0.91	-3.308	114.300	Cea2019	1	0	1.165
Nar	Narmada	973	42	794	1457	0.31	1.49	21.671	72.858	Cea2019	2	1	1.64
Omb	Ombrone	23	165	0	20	0.59	0.12	42.667	11.013	Cea2019	1	1	1.024
Par	Parnaiba	2625	1188	1513	1964	1.60	1.06	-2.800	318.158	Cea2019	1	1	1.086
Raj	Rajang 1	713	212	655	3511	0.67	1.41	2.354	111.517	Cea2019	6	1	1.206

San	Sangu	25	90	18	246	0.37	1.29	22.129	91.888	Cea2019	1	1	1.215
Sen	Senegal	561	2362	608	685	1.47	0.43	16.067	343.525	Cea2019	1	1	1.019
Sep	Sepik	3226	460	420	4816	1.07	0.36	-3.900	144.471	Cea2019	1	0	1.071
Ses	Sesayap	286	2	118	635	0.07	4.22	3.629	117.125	Cea2019	5	0	2.022
Sta	Staaten	75	50	19	124	0.45	0.70	-16.400	141.300	Cea2019	1	1	1.035
Tap	Tapti	515	219	684	614	0.57	1.90	21.133	72.708	Cea2019	4	1	1.519
Wul	Wuli Jiang / Nanliu Jiang	62	40	34	205	0.27	1.41	21.613	109.075	Cea2019	22	0	1.346
Zam	Zambezi	6944	1956	2194	7372	1.30	1.19	-18.800	36.258	Cea2019	7	1	1.131
Bra	Brazos	729	678	3	137	1.10	0.26	28.879	264.625	SS2007	2	1	1.014
ColTX	Colorado, TX	332	714	2	50	1.10	0.23	28.600	264.025	SS2007	10	1	1.015
Cha	Chao	891	5	1418	1265	0.17	0.95	13.617	100.563	SS2007	3	N/A	N/A
Fra	Fraser	1300	0	1102	3721	0.04	1.37	49.158	237.033	SS2007	8	N/A	N/A
Ham	Homathko	47	2	202	122	0.12	1.83	50.929	235.146	SS2007	2	N/A	N/A
Kla	Klamath	171	7446	151	420	2.42	0.95	41.525	235.958	SS2007	1	N/A	N/A
Kli	Klinaklini	19	1	41	158	0.11	1.83	51.092	234.375	SS2007	5	N/A	N/A
Len	Lena	5438	93	550	8492	0.70	0.05	73.151	123.451	SS2007	115	N/A	N/A
Mag	Magdalena	8134	8309	112	7151	2.32	0.15	11.071	285.158	SS2007	7	N/A	N/A
Pec	Pechora	613	37	225	3420	0.31	0.45	68.050	53.950	SS2007	23	N/A	N/A
Pes	Pescara	41	119	0	8	0.69	0.13	42.471	14.225	SS2007	1	N/A	N/A
Rho	Rhone	1605	125	27	1179	0.62	0.09	43.383	4.808	SS2007	2	N/A	N/A
Sqa	Squamish	38	2	204	227	0.12	1.68	49.704	236.821	SS2007	2	N/A	N/A
Tig	Tigris	18362	79	469	1514	0.49	0.60	29.996	48.463	SS2007	5	N/A	N/A
Var	Var	69	331	0	16	0.71	0.10	43.658	7.200	SS2007	1	N/A	N/A
Wai	Waipaoa	6	1190	0	34	1.42	0.46	-38.708	177.938	SS2007	1	N/A	N/A
Zhu	Zhujiang	5386	426	4245	5710	1.00	0.87	22.400	113.258	SS2007	15	N/A	N/A
Gua	Guan He	167	202	785	73	0.79	1.29	34.467	119.783	Cea2019	1	N/A	N/A
Tui	Tuihanpui	161	306	130	64	857.54	0.45	1.130	22.275	Cea2019	1	N/A	N/A
Arn	Arno	80	529	1	41	0.82	0.11	43.683	10.283	SS2007	1	N/A	N/A
Mis	Mississippi	27284	315	713	15126	1.20	0.19	29.113	270.738	SS2007	71	N/A	N/A
Yel	Yellow	7282	307	20	1697	0.91	0.37	37.771	119.175	SS2007	5	N/A	N/A

244

245 **Table S3.** List of field deltas used in this study. Qmx is the maximum monthly discharge
246 from Syvitski and Saito (2007), while all other flux values are taken from the dataset of
247 Nienhuis et al. (2020).

248
249
250
251
252
253
254
255
256
257
258
259

Metric	Statistical test	Goodness of fit	p-value
Roughness (ρ*) (Simulations)	Multiple linear regression ρ* = f(r_{river}, r_{wave}, r_{tide})	$r^2 = 0.62$	$4*10^{-12}$
Roughness (ρ*) (Global deltas)	Multiple linear regression ρ* = f(r_{river}, r_{wave}, r_{tide})	$r^2 = 0.42$	$2*10^{-6}$
Number of Distributary Channels (N_{ch}) (Simulations)	Multiple linear regression N_{ch} = f(r_{river}, r_{wave}, r_{tide})	$r^2 = 0.35$	$2*10^{-5}$
Number of Distributary Channels (N_{ch}) (Global deltas)	Multiple linear regression N_{ch} = f(r_{river}, r_{wave}, r_{tide})	$r^2 = 0.36$	$3*10^{-7}$
Spit Presence/ Absence (S_{PA}) (Simulations)	Multinomial logistic regression S_{PA} = f(r_{river}, r_{wave}, r_{tide})	$\chi^2 = 16.7$	$2*10^{-8}$
Spit Presence/ Absence (S_{PA}) (Global deltas)	Multinomial logistic regression S_{PA} = f(r_{river}, r_{wave}, r_{tide})	$\chi^2 = 38.9$	$6*10^{-2}$ (not significant)

260   **Table S4.** Multiple regressions of flux balance (predictor) versus metric value (response).
261
262
263
264

Model Parameter	Value	Unit
Chezy roughness	65	m^(1/2)/s
Horizontal eddy viscosity	0.0001	m^2/s
Horizontal eddy diffusivity	0.001	m^2/s
Specific density of sediment	2650	kg/m^3
Dry bed density	1600	kg/m^3
Minimum depth for sediment calculations	0.1	m
Threshold sediment thickness	0.05	m
Factor for erosion of adjacent dry cells	0.5	N/A
Transverse bed slope transport factor	1.5	N/A
Wave-related suspended transport factor	0.15	N/A
Wave-related bed-load transport factor	0.15	N/A
Calibration factor (Soulsby-Van Rijn)	1	N/A
Characteristic grain size ratio (Soulsby-Van Rijn)	1.5	N/A
Zo roughness height (Soulsby-Van Rijn)	0.006	m

265   **Table S5.** Additional significant model parameter values.

266

267

Run ID	User-defined parameter being tested (units)	Value	Qriver (kg/s)	Qwave (kg/s)	Qtide (kg/s)	Q (m^3/s)	Nch	ρ*	SPA (0/1 = absent/present)
C120	Flow-wave coupling interval (min)	120 (base value)	198	563.37	12.20	1250	3.8 ± 1.7	1.12 ± 0.02	1
C60	Flow-wave coupling interval (min)	60	198	563.37	12.20	1250	3.3 ± 4	1.10 ± 0.03	1
C30	Flow-wave coupling interval (min)	30	198	563.37	12.20	1250	9.0 ± 3.6	1.12 ± 0.02	1
SF180	Morphological scale factor (N/A)	180 (base value)	198	0.25	12.20	1250	17.6 ± 2.2	1.37 ± 0.03	0
SF90	Morphological scale factor (N/A)	90	198	0.25	12.20	1250	20.4 ± 1.7	1.35 ± 0.03	0
SF60	Morphological scale factor (N/A)	60	198	0.25	12.20	1250	18.3 ± 1.9	1.37 ± 0.02	0
DT0.5	Computational time step (min)	0.5 (base value)	198	0.25	12.20	1250	8.8 ± 3.4	1.37 ± 0.03	0
DT0.25	Computational time step (min)	0.25	198	0.25	12.20	1250	9.1 ± 1.2	1.34 ± 0.02	0
DT0.1	Computational time step (min)	0.1	198	0.25	12.20	1250	10.3 ± 2.2	1.32 ± 0.03	0

268 **Table S6.** Model parameter sensitivity tests.

269

270